# Poincaré section analysis of chaotic rotation in the orbit of Hyperion

Candidate Number: 24669

Department of Physics, University of Bath, Bath BA2 7AY, United Kingdom

March 14, 2022

**Abstract**

The 7th moon of Saturn, Hyperion is well known for its ashperical shape and resulting chaotic rotation. This report presents a model of the orbit of Hyperion in two dimensions that considers its asphericity and orientation, which predicts chaotic behaviour in rotation and angular frequency over several orbits. A computational method of generating datasets from the equations of motion is developed for use in a Poincaré section of the phase space of the rotational states of Hyperion. Analysis of the Poincaré section reveals a 'chaotic sea' of rotational states bounded by unstable periodic sets of states. Further examination reveals 'islands' corresponding to unstable quasi-periodic patterns within the chaotic region.

A brief comparison with aspherical Martian moons Phobos and Deimos are made using the same model which reveals...

# Introduction

Hyperion, first discovered in 1848 by William Lassell[1], is one of the largest aspherically shaped bodies in the solar system (dimensions $410 \times 260 \times 220$ km)[1], and the only regular planetary satellite in the solar system known to not be tidally locked [1]. Its orbit is also highly eccentric with eccentricity $e = 0.232$ and semi major axis $a = 1.501 \times 10^9$ m [1]. There are other possible orbital modes that are tidally locked but rotate in a nonsynchronous fashion; for example Mercury is tidally locked with a 3:2 spin orbit resonance [2], that is, for every two revolutions about the sun, it revolves on its axis exactly three times.

Such resonant states are predicted to contribute to the motion of hyperion, J. Wisdom *et al* (1983) modelled the spin of hyperion as a Hamiltonian system, which consequently predicts the existence of a large chaotic zone in the phase space due to perturbation effect of nonsynchronous quasi-periodic unstable rotational states (described as resonant or $p$ states) on each other [3]. This was later shown to fit observational data by J. Klavetter in 1989 [4] [5]. Since these findings many have studied the chaotic motion of Hyperion inlcuding P. Boyd *et al*, who developed a 'method of close returns' for analysing the chaotic motion relative to unstable periodic orbits in the chaotic regions of phase space [6], where states are attracted to and repelled by these orbits.

In our model of the orbit of Hyperion, we employ a two dimensional description of orbit derived from Newtonian mechanics[**?**], and a correction to include angle of orientation and corresponding angular frequency $(\theta(t), \omega(t))$. This results in a set of six coupled ODEs with corresponding initial conditions, in particular, we will examine the effects of taking different initial conditions of rotational state $(\theta(0), \omega(0))$ on the rotation over many orbits by solving the initial value problem numerically by Runge-Kutta-Fehlberg 45 (rkf45) approximation which is accurate to 5th order. To examine the results a Poincaré section of $\omega/\omega_H$ against $\theta$ is taken, where $\omega_H$ is the angular frequency of the orbit of Hyperion about Saturn.

# The model

## Classical orbit

The model for position and velocity of Hyperions orbit follows directly from Newtonian mechanics, we limit the motion to the x-y plane. The position $(x_H, y_H)$ and velocity $(vx_H, vy_H)$ of Hyperion are described by the four coupled ODEs

$$\frac{dx_H}{dt} = vx_H, \quad \frac{dy_H}{dt} = vy_H, \tag{1}$$

$$\frac{dvx_H}{dt} = -\frac{GMx_H}{\left(x_H^2 + y_H^2\right)^{3/2}}, \frac{dvy_H}{dt} = -\frac{GMy_H}{\left(x_H^2 + y_H^2\right)^{3/2}}, \tag{2}$$

where $M = M_{\text{Sat}} + M_H$ with $M_{\text{Sat}} = 5.6832 \times 10^{26}$ kg and $M_H = 5.5855 \times 10^{18}$ kg the masses of Saturn and Hyperion respectively. $G = 6.67408 \times 10^{-11}$ Nm$^2$kg$^{-2}$ is the gravitational constant. For an orbit of eccentricity $e = 0.232$ these ODEs are paired with initial conditions

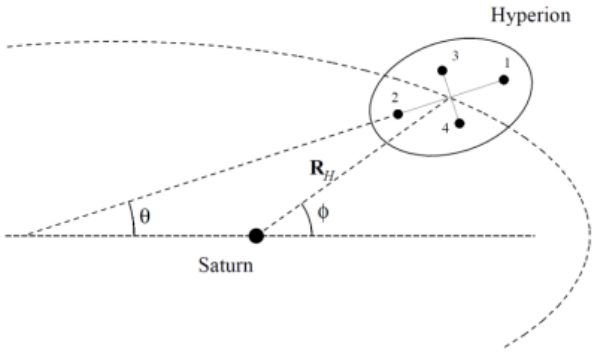


Figure 1: Diagram of the orbit of Hyperion in the x-y plane with angle $\phi$ to the line of periapse (major axis) and radius $R_H$. Shown are the four equal masses from which the axes of moments of inertia $I_1, I_2$ are determined. The orientation $\theta$ of Hyperion is defined as the angle made between the axis of smallest moment of inertia and the line of periapse. This diagram is taken from the project assignment sheet by S. Crampin [**?**].

$$x_H(0) = a(1-e), \quad y_H(0) = 0, \tag{3}$$

$$vx_H(0) = 0, \quad vy_H(0) = \sqrt{\frac{GM(1+e)}{a(1-e)}}, \tag{4}$$

where $a = 1.501 \times 10^9$ m is the semi-major axis of orbit. These initial conditions ensure an elliptic orbit clockwise in x-y starting at perihelion. From Keplar's laws we find the period of the orbit $T_H = \sqrt{4\pi^2 a^3/GM} = 1.876 \times 10^6$ s from which we can determine the angular frequency $\omega_H = 2\pi/T_H = 3.349 \times 10^{-6}$ rad s$^{-1}$.

This is a simple classical model of orbit that doesn't consider the rotation of Hyperion, we can quantify error in our numerical solution by considering the difference in position and velocity at perihelion after $n$ orbits, which should stay constant. Analysis of this difference shows that after $n = 100$ orbits the difference in magnitude of position and velocity are $10^{-6}\times$ the magnitudes of our initial conditions. We will take this error as negligible as in our analysis we don't generate data for greater than 100 orbits. If a very large number of orbits were modelled this error could be far greater.

## Asphericity and rotation

The model is extended to consider the asphericity of Hyperion. Because of its asphericity it we can define its orientation $\theta$. Our model is simplified by restriction of motion the x-y plane of orbit, so its spin axis is in the $z$, normal ot the orbit plane, we also take this to be the axis with the largest mass moment of inertia $I_3$. The orientation of Hyperion $\theta$ is then defined to be the angle between its smallest moment of inertia and the line of periapse of its orbit, this is more clearly shown in FIG. 1.

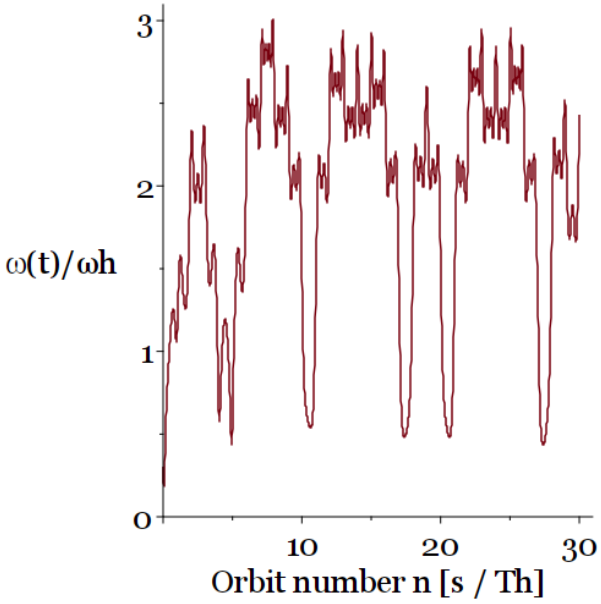


Figure 2: Plot of angular frequency $\omega(t)$ against time (number of orbits $T_H$) of Hyperion for initial conditions $\omega(0) = 0.3\omega_H \theta(0) = \pi/7$ where $\omega_H$ is the angular frequency of Hyperions orbit about Saturn. There is chaotic behaviour with some seemingly recurring patterns, these can be interpreted as states of rotation that are more likely to occur in this chaotic system.

The dynamics of the orientation $\theta$ are found by substituting the actual mass distribution with four equal masses in the x-y plane such that the lines of seperation between these masses align with the axes of moments of inertia $I_1, I_2$.

We define the asphericity factor of Hyperion to be $\beta = \sqrt{3(I_2 - I_1)/I_3} = 0.89$. By examining the contributions to torque from our model we can retrieve an expression for the net torque $T$ about the axis of rotation aligned with $z$. This equivalent to the change in angular momentum $T = I_3 \frac{d^2\theta}{dt^2}$, and hence

$$\frac{T}{I_3} = \frac{d^2\theta}{dt^2} = -\frac{GM_{sat}\beta^2}{2R_H^3} \sin 2(\theta - \phi) \tag{5}$$

Where $\phi$ is the angle of the orbit around Saturn against the line of periapse and $R_H = \sqrt{x_H^2 + y_H^2}$ is the radius of orbit. We then use two coupled first order ODEs to describe the rotation of Hyperion

$$\frac{d\theta}{dt} = \omega, \quad \frac{d\omega}{dt} = -\frac{GM_{sat}\beta^2}{2R_H^3} \sin 2(\theta - \phi). \tag{6}$$

The initial conditions of $\theta$ and $\omega$ are not known and will serve as our independent variables in further analysis.

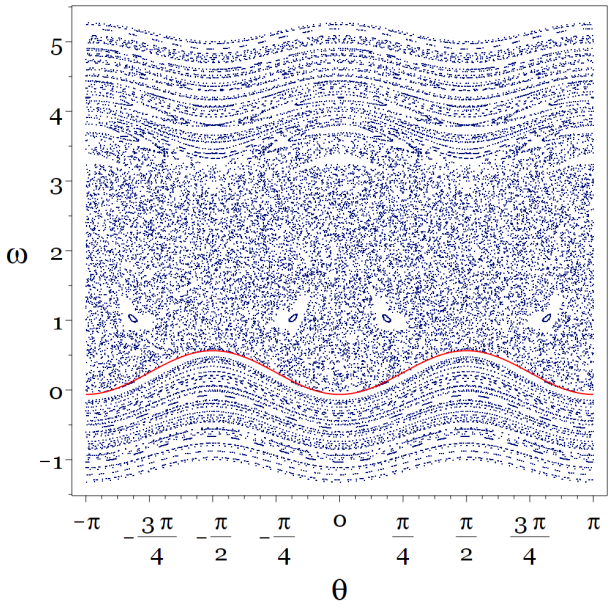


Figure 3: Poincaré section plot of $\omega/\omega_H$ against $\theta$ at $t = nT_H$ for $n$ orbits in the interval $[0, 50]$ with initial conditions $\theta(0) \in [0, 2\pi], \omega(0) \in [-1, 5\omega_H]$ with intervals of $0.1\pi$ and $0.3\omega_H$ respectively (33201 points). The majority of the plot is dominated by a large 'chaotic sea' bounded by periodic patterns of states $\omega = A\cos(2\theta)+B$ for constants $a, b$ (highlighted in red). There are also notable 'islands' of states in the chaotic sea where there are voids with a distinct lack of rotational states a dense region of states within.

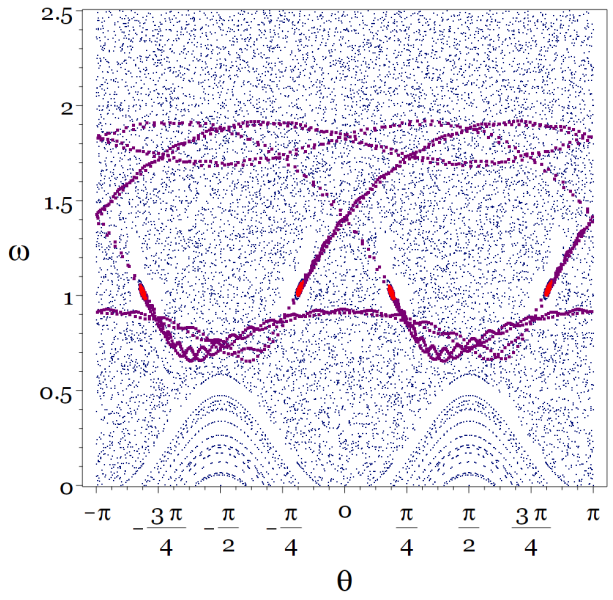


Figure 4: Poincaré section plot for initial conditions $\theta(0) = -13\pi/16, -3\pi/16, 3\pi/16, 13\pi/16$, $\omega(0) = \omega_H$ and $n = 100$ (404 points, red). The states remain firmly in the bounds of the 'islands' in the chaotic sea. However for initial condition $\theta(0) = -13\pi/16, \omega(0) = \omega_H$ starting in just one island, over many more orbits $n = 1500$ (1501 points, purple) the orbit evolves to reveal a periodic unstable nonsynchronous set of states within the chaotic region (FIG 3, blue).

A plot of $\omega(t)$ against $t$ for some initial conditions $\omega(0) = 0.3\omega_H \theta(0) = \frac{\pi}{7}$ seen in FIG. 2 displays some chaotic behaviour, that is, random behaviour in a deterministic system. Because of the chaotic nature of this motion, it is not possible to distinguish error from chaos in any measurements of $\theta$ and $\omega$.

## Poincaré section

To gain further insight on this chaotic behavior in FIG 3 we take a Poincaré section of $\omega(t)/\omega_H$ against $\theta(t)$ modulo $2\pi$ at perihelion $t = nT_H$ for $n \in N$. The Poincaré section is taken with $n = 1 \cdots 100$ orbits and initial conditions $\theta(0) \in [0, 2\pi], \omega(0) \in [-1, 5\omega_H]$ with intervals of $0.1\pi$ and $0.2\omega_H$ respectively for a total of 33,201 sampled points. FIG 3 and the procedure poincare() that generates these points are detailed in the appendix. Qualitatively, we observe a large 'chaotic sea' of rotational states bounded by periodic sets of states $\omega(t) = A\cos(2\theta) + B$ for constants $A, B$. These periodic sets of states continue outside of the chaotic sea in a discrete way, forming 'bands' of rotational states. Finally there are distinct 'islands' in the chaotic sea around $\omega = 0$ and $\theta = -13\pi/16, -3\pi/16, 3\pi/16, 13\pi/16$ where at each island there is a small dense region of states within a surrounding empty region.

To further examine these periodic patterns in FIG **??** Poincaré sections are taken with initial conditions in these regions of interest. Firstly, in FIG **??** with initial conditions $\theta(0) = -13\pi/16, -3\pi/16, 3\pi/16, 13\pi/16, \omega(0) = \omega_H$ around the islands at we see four distinct sets of states with the same orientation $\theta$ over a very low range of angular frequency $\Delta\omega \approx 0.08\omega_H$. In FIG **??** a plot is taken with just one initial condition at the island corresponding to $\theta(0) = -13\pi/16$ over a large number of orbits $n = 1500$, we reveal an unstable periodic set of states inside the chaotic region. This set of states visits the four other islands after several orbits. It is likely that this corresponds to one of the nonsynchronous $p$ states inside the chaotic region discussed by J. Wisdom *et al.* However due to the larger number of orbits measured, the error in position and velocity could be large enough to effect the states seen, especially due to their high dependence on initial conditions.

In FIG 5a when initial conditions are taken across $\omega(0) = -\omega_H$ the result is a set of six distict 'bands' of rotational states. The primary similarity between these bands is that they have the form $A\cos(2\theta) + B$, and that they all cross the line $\omega(\theta) = -\omega_H$, with the highest and lowest bands having their minima and maxima respec-

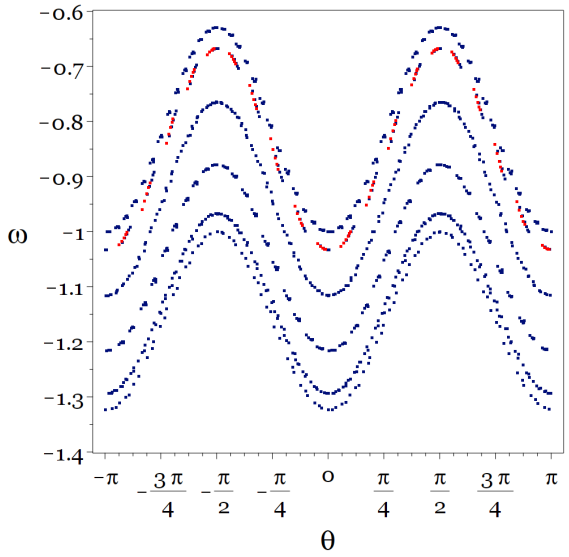


(a) Poincaré section plot for initial conditions $\theta(0) \in [0, \pi]$ with interval $\pi/10$, $\omega(0) = -\omega_H$ and $n = 100$ (1111 points). There are six distinct 'bands' of rotational states of form $A\cos(2\theta)+B$. Highlighted in red is the band from initial condition $\theta(0) = \pi/10$

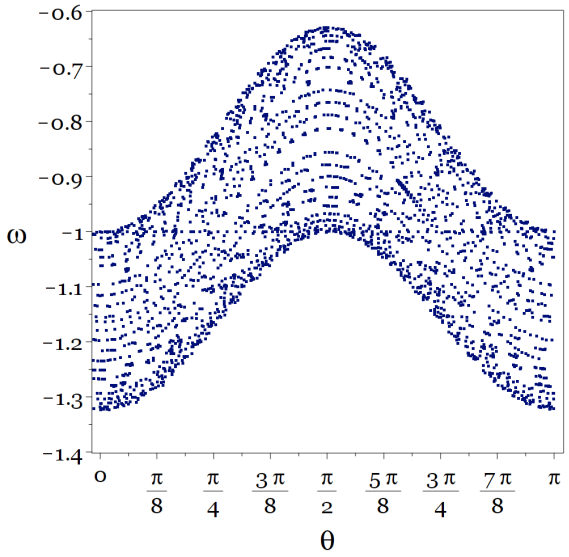


(b) Poincaré section plot restricted to $\theta = [0, \pi]$ for initial conditions $\theta(0) \in [0, \pi]$ with interval $\pi/50$, $\omega(0) = -\omega_H$ and $n = 100$ (5151 points). When more samples are taken the bands become less distinct.

Figure 5: Poincaré section plots of $\omega(t)/\omega_H$ against $\theta(t)$ at $t = nT_H$ for varying initial conditions $\omega(0), \theta(0)$ and over number of orbits $n$. Initial conditions are selected to highlight regions of interest.

tively almost exactly at $-\omega_H$. This suggests that states outside of the chaotic region are more stable and generally stick to a set range of angular frequencies.

We take a larger sample of points from more initial conditions $\theta(0) \in [0, \pi]$ with interval $\pi/50$ and $\omega(0) = -\omega_H$ in FIG 5b. We see that the region bounded by the upper and lower bands in FIG 5a is now full of many sinusoidal patterns, however they are much harder to distinguish, and states near the upper and lower bounds begin to look looks chaotic. Interestingly at $\theta \approx 21\pi/32, \omega \approx -0.95\omega_H$ there is a particularly dense region of states. The fact that chaos can be found in the fine strucure of a Poincaré plot outside of the chaotic sea is supported by the literature []

This is further supported by additional computations excluded from this written report but that are accessible in the accompanying worksheet that show for a single initial condition state, for small $n$ 100 a band can be isolated and is stable, however as the orbit evolves to say, $n$ 10000 it becomes chaotic, but is still bounded in $\omega$ to the same region as the isolated band. This computation of course may be heavily effected by error in computing values for such a large $n$.

# Comparison with a less eccentric orbit

To develop our insight on the effects of orbit eccentricity $e$ and the asphericity $\beta$ on the rotational states of an orbit we construct a toy model which substitutes the eccentricity of orbit and apshericity Hyperion to that of the Martian moons Deimos and Phobos. All other parameters, in particular the masses $M_{\text{Sat}}, M_H$ involved and the semi-major axis $a$ are preserved.

mars graphs discussion here

# Conclusion

begin conclusion

poincare results

mars results

End conclusion

# Acknowledgements

We would like to acknowledge the contributions of Dr S. Crampin for his code and resources on which this model is based, and N. Roberts for providing the latex template used in the creation of this report.

# References


[1] NASA, “Hyperion in depth,” 2019. Available from https://solarsystem.nasa.gov/moons/saturn-moons/hyperion/in-depth/ [Accessed 16 December 2021].

[2] G. Colombo and I. I. Shapiro, “The Rotation of the Planet Mercury,” *Astrophysics Journal*, vol. 145, p. 296, jul 1966.

[3] J. Wisdom, S. J. Peale, and F. Mignard, “The chaotic rotation of hyperion,” *Icarus*, vol. 58, pp. 137–152, 1984.

[4] J. J. Klavetter, “Rotation of Hyperion. I. Observations,” *Astronomical Journal*, vol. 97, p. 570, feb 1989.

[5] R. P. Binzel, J. R. Green, and C. B. Opal, “Chaotic rotation of hyperion?,” *Nature*, vol. 320, pp. 1476–4687, 1986.

[6] P. Boyd, G. Mindlin, G. Robert, and S. Hernán, “Topological analysis of chaotic orbits: Revisiting hyperion,” *The Astrophysical Journal*, vol. 431, 09 1994.

# Appendix

The numerical... was done using maple

Try to make this single width

Eqns, ICs

```
Eqns := {diff(vxh(t), t) = -G*M*xh(t)/Rh(t)^3,
         diff(vyh(t), t) = -G*M*yh(t)/Rh(t)^3,
         diff(xh(t), t) = vxh(t),
         diff(yh(t), t) = vyh(t)};

ICs := {vxh(0) = 0,
        vyh(0) = sqrt(G*M*(1 + e)/(a*(1 - e))),
        xh(0) = a*(1 - e),
        yh(0) = 0};
```

with rotation TIDY THIS

```
Eqns_rotation := Eqns union {diff(omega(t), t) = -G*M_sat*beta^2*(xh(t)*sin(theta(t)) - yh(
diff(theta(t), t) = omega(t)};
```

Code developed for use in taking Poincaré sections: The *poincare()* procedure, written in maple, takes inputs for *thetaO, omegaO*| the initial conditions for rotation and *n* the number of orbits to generate data for. *thetaO* and *omegaO* should be given as lists of values, for a single intitial condition lists of one item can be passed to the procedure.*poincare()* will then find each state $(\theta(t) \mathrm{mod} 2\pi, \omega(t)/\omega_H)$ where $t = nT_H$ for $n$ from 0 to $n$ at every combination of initial conditions $\theta(0) =$ thetaO and $\omega(0) =$ omegaO it recieves. The resulting data is output as an array of touples.

```
poincare := proc(thetaO::list, omegaO::list, n::nonnegint)
  local data, local_ICs, soln, omeg, thet, i, j, k;
  global wh, Eqns_rotation, ICs, ICs_rotation;
  data := [];
  for i in thetaO do
    for j in omegaO do
      local_ICs := ICs union {omega(0) = j, theta(0) = i};
      soln := dsolve({Eqns_rotation[], local_ICs[]}, numeric, maxfun = -1, range = 0 .. (n +
      for k from 0 to n do
        omeg := rhs(soln(k*Th)[2])/wh;
        thet := frem(rhs(soln(k . Th)[3]), evalf(2*Pi));
        data := [op(data), [thet, omeg]];
      end do;
    end do;
  end do;
  return data;
end proc:
```

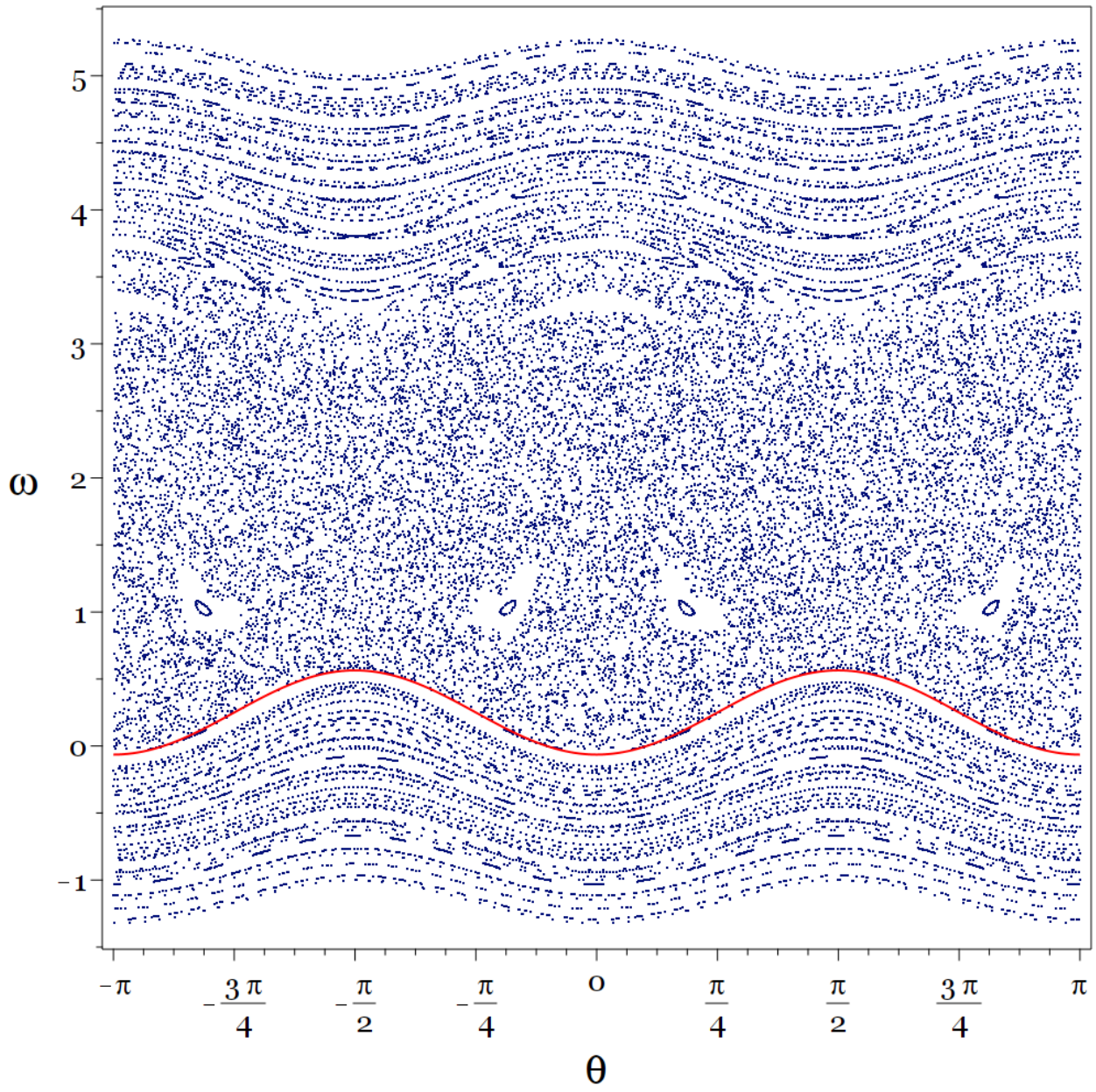


Figure 6: Poincaré section plot of $\omega/\omega_H$ against $\theta$ at $t = nT_H$ for $n$ orbits in the interval $[0, 50]$ with initial conditions $\theta(0) \in [0, 2\pi], \omega(0) \in [-1, 5\omega_H]$ with intervals of $0.1\pi$ and $0.3\omega_H$ respectively (33201 points). The majority of the plot is dominated by a large 'chaotic sea' bounded by periodic patterns of states $\omega = A\cos(2\theta) + B$ for constants $a, b$ (highlighted in red). There are also notable 'islands' of states in the chaotic sea where there are voids with a distinct lack of rotational states a dense region of states within.